nature neuroscience

Sensory and decision-related activity propagate in a cortical feedback loop during touch perception

Sung Eun Kwon, Hongdian Yang, Genki Minamisawa & Daniel H O'Connor

The brain transforms physical sensory stimuli into meaningful perceptions. In animals making choices about sensory stimuli, neuronal activity in successive cortical stages reflects a progression from sensation to decision. Feedforward and feedback pathways connecting cortical areas are critical for this transformation. However, the computational functions of these pathways are poorly understood because pathway-specific activity has rarely been monitored during a perceptual task. Using cellular-resolution, pathway-specific imaging, we measured neuronal activity across primary (S1) and secondary (S2) somatosensory cortices of mice performing a tactile detection task. S1 encoded the stimulus better than S2, while S2 activity more strongly reflected perceptual choice. S1 neurons projecting to S2 fed forward activity that predicted choice. Activity encoding touch and choice propagated in an S1–S2 loop along feedforward and feedback axons. Our results suggest that sensory inputs converge into a perceptual outcome as feedforward computations are reinforced in a feedback loop.

Perceptual decisions involve propagation and transformations of sensory signals across multiple hierarchically organized cortical areas[1]. Feedback projections are a ubiquitous feature of cortical organization[2] and are implicated in numerous functions, such as contextual modulation of perception, attention, sensory expectation, and perceptual learning[3,4]. Feedback to primary sensory cortical areas is even hypothesized as essential for sensory awareness[5]. Sensory cortex feedforward and feedback connections form recurrent neural networks. Recurrent networks can exhibit complex dynamics and perform sophisticated computations, such as by forming content-addressable memory networks for pattern completion[6], amplification of input signals[7–9], and the maintenance of neural activity over timescales longer than permitted by the biophysics of individual neurons[10].

How feedforward and feedback cortical dynamics mediate the transformation from raw sensory input to actionable interpretations of the sensory world (that is, to perceptual decisions) is not understood. This is largely due to the difficulty of using traditional methods to measure neural activity within defined synaptic pathways during behavior. Progress requires theoretical work on recurrent networks to be embodied in specific circuitry[11]. *In vivo* two-photon imaging, combined with strategies to mark axons or neurons by their projection patterns, allows the activity of specific cortico-cortical pathways to be monitored[12] during behavior[13–18]. Here we used a combination of pathway-specific imaging and optogenetics to investigate the perception-related dynamics of a recurrent network between primary and secondary somatosensory cortex.

RESULTS

We trained mice to perform a head-fixed tactile detection task in which they reported by licking or withholding licking whether a single whisker received a brief sinusoidal deflection (20 Hz, 0.5 s, ~800 degrees s^{-1} peak speed; **Fig. 1**). Trial outcomes comprised a mixture of successful detections ('hits') and failed detections ('misses') following stimulus delivery, as well as correct responses ('correct rejection') and incorrect responses ('false alarms') in the absence of the stimulus (**Fig. 1c** and **Supplementary Fig. 1**). The relationship between touch perception and responses across large-scale populations of cortical neurons remains poorly understood, even for S1. Anatomy[19,20] and physiology in anesthetized or narcotized rodents[21–23] suggest that mouse S2 is a higher, or more integrative, cortical area than S1. However, responses of rodent S2 neurons during tactile behavior are nearly entirely unexplored (but see refs. 24,25). We thus began by mapping responses to stimulation of a single whisker across whisker representation areas of S1 and S2, in separate mice, as they performed the detection task.

Mapping activity in S1 and S2 during tactile detection

We used *in vivo* two-photon imaging of GCaMP6 genetically encoded calcium indicators[26] to measure spiking-related fluorescence signals from the cell bodies of layer 2/3 (L2/3) neurons. For our single-whisker stimuli, we found that 37.0 ± 2.3% (mean ± s.e.m. across mice) of neurons in S1 and 23.6 ± 4.1% of neurons in S2 gave task-related responses ('responsive' neurons; Online Methods; **Fig. 1h**). Thus, behaviorally relevant whisker stimulation is represented robustly in whisker regions of both S1 and S2. We limited subsequent analyses to responsive neurons, except where noted, and used responses occurring in a time window (0.25 s after stimulus onset) preceding the typical reaction times (**Fig. 2a**,**b**). The end of this window precedes 96.5% of reaction times (**Supplementary Fig. 1**).

Overall, responses of individual neurons to the whisker stimulus tended to be larger in S1 than in S2 (S1: hit: 0.036 ± 0.006 $\Delta F/F_0$; miss: 0.024 ± 0.006 $\Delta F/F_0$; S2: hit: 0.029 ± 0.016 $\Delta F/F_0$; miss: 0.015 ± 0.008 $\Delta F/F_0$; mean ± s.e.m. across mice; $z = 3.19$, $P = 0.0014$, for comparison of hits; $z = 7.46$, $P = 8.38 \times 10^{-14}$ for comparison of misses; 1,370 neurons in S1; 607 neurons in S2; Wilcoxon rank sum tests; **Fig. 2a**,**b**), suggesting a more robust representation of the tactile stimulus in S1.

The Solomon H. Snyder Department of Neuroscience, Kavli Neuroscience Discovery Institute, Brain Science Institute, The Johns Hopkins University School of Medicine, Baltimore, Maryland, USA. Correspondence should be addressed to D.H.O. (dan.oconnor@jhmi.edu).

Received 10 May; accepted 5 July; published online 20 July 2016; doi:10.1038/nn.4356

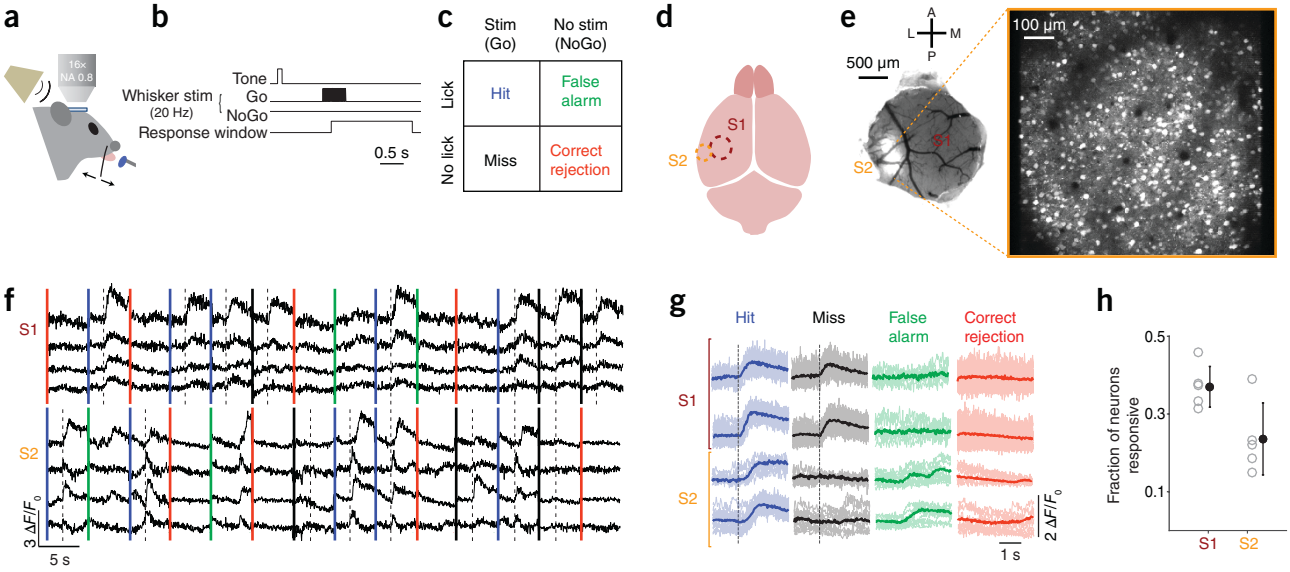

Figure 1 Cellular resolution imaging of population activity in S1 and S2 during tactile detection. (**a**) Experimental setup. Mice were trained to report detection of single-whisker deflections by licking a port for a liquid reward. Activity of L2/3 neurons in the whisker area of S1 or S2 was monitored by two-photon calcium imaging. (**b**) Trials began with an auditory cue. On 50% of trials ('Go' trials), a single whisker was deflected with a sinusoidal waveform (0.5 s, 20 Hz). The whisker was not deflected on the other 50% of trials ('NoGo' trials). Trial outcome was determined by lick responses occurring during a response window. (**c**) Four possible trial outcomes based on the stimulus condition (present versus absent) and the animal's response (lick versus no-lick). (**d**) Schematic of brain areas monitored by two-photon imaging. S1 (brown) or S2 (orange) were identified using intrinsic signal optical imaging. (**e**) Left, view through a cranial imaging window implanted over S1 and S2. GCaMP6 expression (white) is evident in S2. Right, example field of view for two-photon calcium imaging (max projection through time for a trial). (**f**) Example GCaMP6 fluorescence traces concatenated across trials from S1 and S2 imaging sessions. Vertical colored lines indicate start of each trial (blue, hit; black, miss; green, false alarm; red, correct rejection). Dashed lines, onset of whisker stimulus. (**g**) Example fluorescence traces (thin lines) and means (thick) showing two S1 and two S2 neurons (one neuron per row). Traces are grouped and colored by trial type. Dashed lines, onset of whisker stimulus. (**h**) Fraction of neurons that were task responsive in S1 or S2, for individual mice (gray circles) and means (black; ± s.e.m.).

Touch-evoked activity in both S1 and S2 predicted the subsequent perceptual choice of the mouse. Responses on hit trials were larger than on miss trials in both S1 and S2 (hit – miss mean ± [95% confidence interval, CI] for evoked $\Delta F/F_0$: S1: 0.013 ± [0.008, 0.019] $\Delta F/F_0$; S2: 0.012 ± [0.010, 0.023] $\Delta F/F_0$; **Fig. 2a**,**b**). Thus, activity in each area predicted whether the mouse would succeed or fail to detect an identical stimulus. In the absence of a whisker stimulus, activity was higher on false alarm trials than on correct rejections in S2 (false alarm – correct rejection mean ± [95% CI]: S1: 0.000 ± [–0.006, 0.005] $\Delta F/F_0$; S2: 0.006 ± [0.009, 0.011] $\Delta F/F_0$; **Fig. 2a**,**b**). To quantify modulation of neuronal activity by behavioral choice, we normalized responses of individual neurons to the mean hit response, in order to account for overall differences in evoked activity between the two areas. We observed a smaller normalized miss response in S2 (**Fig. 2c**). Thus, individual neurons were more modulated by choice in S2 than in S1.

Trial-by-trial coding by single neurons and populations

Ideal observer analysis is frequently used to correlate the trial-by-trial activity of single sensory cortex neurons with stimuli and perceptual choices[27,28]. To investigate stimulus and choice encoding by single neurons, we first calculated stimulus probability (SP). SP gives the probability with which an ideal observer could correctly categorize the stimulus condition (present versus absent) of a trial on the basis of the response of a single neuron (Online Methods). We also calculated detect probability (DP, which is mathematically identical to choice probability[27] but often renamed in the context of detection tasks[29]). DP is the probability with which an ideal observer could correctly categorize the behavioral choice of the mouse on a single trial (in our case, lick versus no-lick) on the basis of the response of a neuron[27]. We observed robust (above chance level, >0.5) SP and DP in S2 as well as S1 (**Fig. 2d**). S1 trended toward having a higher fraction of neurons with significant SP ('SP neurons', defined as neurons whose 95% confidence interval for SP did not include 0.5; 49.7 ± 3.1% of responsive neurons in S1 versus 32.2 ± 3.4% of responsive neurons in S2; mean ± s.e.m. across mice; P = 0.24, permutation test; **Supplementary Fig. 2**). The distribution of SP showed larger values overall in S1 than in S2 (**Fig. 2d**). The distribution of DP was similar in the two cortical areas, despite the weaker stimulus representation in S2 (**Fig. 2d**). The ratio of DP to SP for neurons in S2 was higher than for neurons in S1 (**Fig. 2d**), consistent with a greater choice-related modulation of S2 responses.

Choice-related activity is thought to depend on correlations among neuronal responses, which in turn reflect cortical topography[29,30]. However, while detect (or choice) probability is frequently quantified, its cellular-resolution organization within cortex is unknown. We therefore mapped SP and DP across S1 and S2 in separate mice (**Fig. 2e**–**j**). First, we tested whether SP neurons and DP neurons (defined as a neuron with 95% confidence interval for DP not including 0.5) were clustered. In S1, pairwise distances among SP neurons were smaller than pairwise distances among all neurons (median distances: 243 µm versus 281 µm; **Fig. 2g**). Clustering of SP neurons is expected as a result of the somatotopy of barrel cortex. Notably, DP neurons were also clustered in S1, with smaller pairwise distances than expected based on the distribution for all neurons (median distances 256 µm versus 281 µm; **Fig. 2g**). In S2, neither SP nor DP neurons formed obvious clusters (**Fig. 2h**).

We next examined how SP and DP were distributed as a function of distance from the center of the somatotopic representation of the stimulated whisker. In S1, this somatotopic representation corresponds to the stimulated whisker's barrel column. We estimated the center of

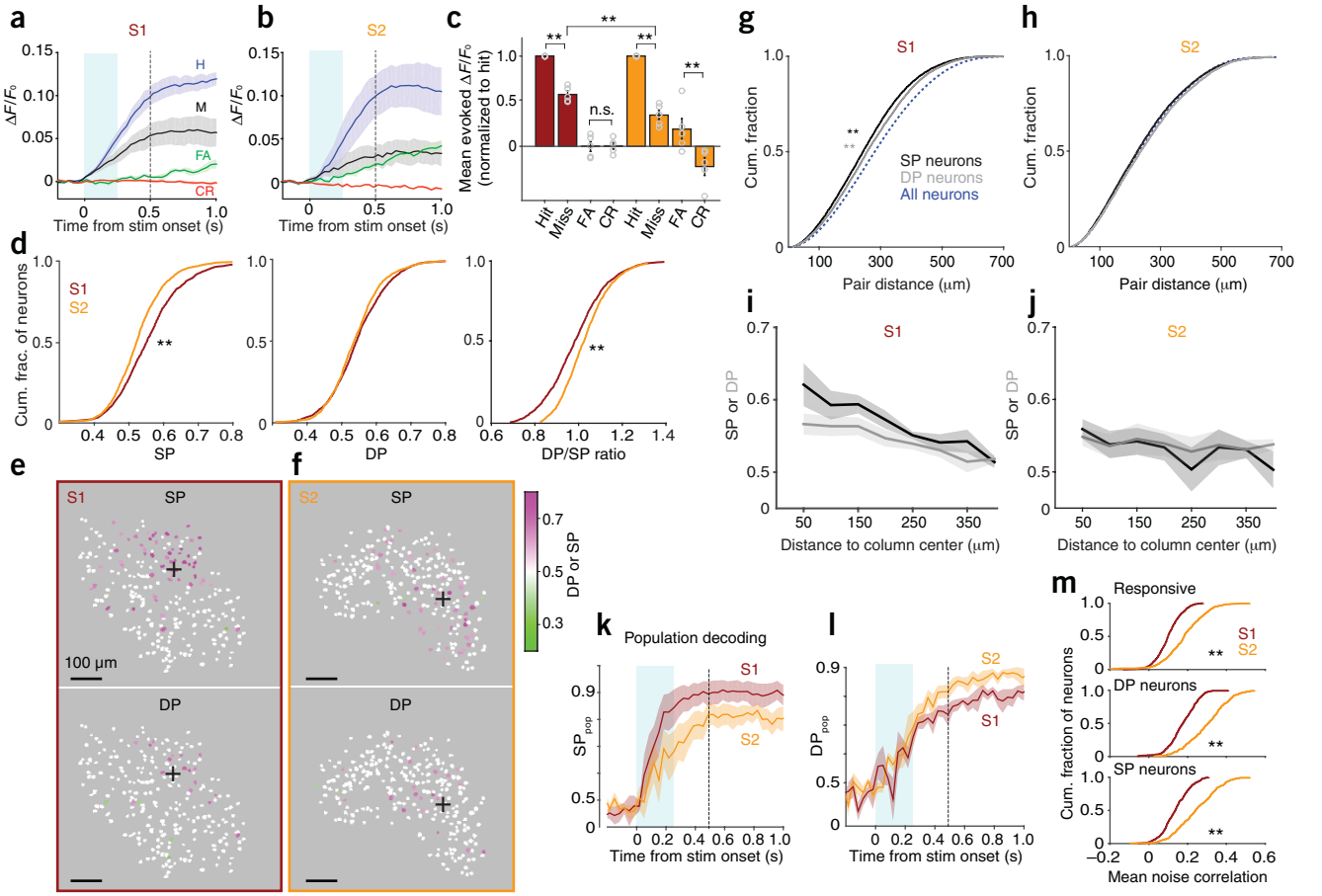

Figure 2 Coding of stimulus and choice in S1 and S2. (**a**) Activity (mean ± s.e.m. $\Delta F/F_0$ across mice) averaged across hit (H; blue), miss (M; black), false alarm (FA; green) and correct rejection (CR; red) trials from S1 imaging sessions (12 sessions, 5 mice, 274 ± 52 neurons per mouse; mean ± s.e.m.). Evoked $\Delta F/F_0$ responses on hits were larger than on misses ($t_{(1,369)} = 16.79$, $P = 1.17 \times 10^{-57}$; 1,370 neurons; paired *t*-test). Cyan shading, first 0.25 s after stimulus (stim) onset, which preceded 96.5% of first licks. Dashed line, last time point before median first-lick time. (**b**) Same as **a** for S2 (11 sessions, 5 mice, 103 ± 26 neurons per mouse). Evoked $\Delta F/F_0$ responses on hits were larger than on misses ($t_{(606)} = 20.32$, $P = 2.22 \times 10^{-70}$; 607 neurons; paired *t*-test). In S2, evoked $\Delta F/F_0$ responses on false alarms were larger than on correct rejections ($t_{(606)} = 4.07$, $P = 5.33 \times 10^{-5}$; paired *t*-test). (**c**) Mean evoked $\Delta F/F_0$ responses normalized to hits across individual neurons in S1 and S2 (mean ± s.e.m. across mice; circles show individual mice). For both S1 and S2 neurons, responses on misses were smaller than on hits (miss/hit ratio: S1: 0.57 ± 0.04; $z = 22.3$, $^{**}P = 1.73 \times 10^{-110}$; 1,370 neurons; S2: 0.32 ± 0.05; $z = 18.84$, $^{**}P = 3.76 \times 10^{-79}$; 607 neurons; Wilcoxon sign rank tests), with stronger modulation for S2 compared with S1 ($z = 7.46$, $^{**}P = 8.38 \times 10^{-14}$; Wilcoxon rank sum test). (**d**) Cumulative histograms (means across mice) of SP (left), DP (middle) and DP/SP ratio (right) for all (responsive and nonresponsive) neurons in S1 (brown) and S2 (orange). DP/SP ratio was higher in S2 than in S1 (medians: 1.01 versus 0.97; $D = 0.093$, $^{**}P = 1.96 \times 10^{-7}$; 2,490 S1 and 1,471 S2 neurons; Kolmogorov-Smirnov test); SP was higher in S1 than in S2 (medians: 0.55 versus 0.52; $D = 0.063$, $^{**}P = 0.0013$; Kolmogorov-Smirnov test) while DP was similar ($D = 0.044$, $P = 0.056$; Kolmogorov-Smirnov test). (S1: 12 sessions, 5 mice, 498 ± 74 neurons per mouse; S2: 11 sessions, 5 mice, 294 ± 47 neurons per mouse). (**e**) Maps from one mouse showing distributions of stimulus- and decision-encoding neurons in S1. White neurons are those whose SP or DP 95% confidence intervals included 0.5. Responsive and nonresponsive neurons are included. Black plus signs mark the center of the somatotopic column of the stimulated whisker. (**f**) Same as **e** for S2. (**g**) Cumulative histograms of pairwise distances among SP neurons (black), DP neurons (gray), and all neurons (dashed blue; responsive and nonresponsive) in S1. Both SP and DP neurons had smaller pairwise distances among themselves compared with all neurons (both $^{**}P < 5 \times 10^{-5}$; 26,898 SP, 12,387 DP, and 431,962 all-neuron pairs; bootstrap). (**h**) Same as **g** for S2. (**i**) Mean SP (black) and DP (gray) values averaged across all neurons (8 bins of 50 μm; ± s.e.m.) as a function of distance from the center of the somatotopic column representing the stimulated whisker in S1. SP and DP both decreased with distance from the column center (SP: –0.028 per 100 μm; DP: –0.017 per 100 μm; test of zero slope: $F_{(1,74)} = 54.84$, $P = 1.711 \times 10^{-10}$; difference in slopes for SP and DP: $F_{(1,74)} = 3.58$, $P = 0.062$; 78 binned values total from 5 mice; ANCOVA). (**j**) Same as **i** for S2 (test of zero slope: $F_{(1,54)} = 3.11$, $P = 0.083$; difference in slopes for SP and DP: $F_{(1,54)} = 0.92$, $P = 0.342$; 58 values from 5 mice). (**k**) Performance of a classifier (mean ± s.e.m. across mice) in decoding the stimulus condition from population activity at each time point reached higher levels for S1 (84 ± 7% correct by 0.25 s after stimulus (stim.) onset, and 89 ± 5% by the median reaction time of 0.52 s) compared with S2 (68 ± 8% correct by 0.25 s, 82 ± 4% by 0.52 s; performance diverged by 0.32 s: $U = 76$, $P = 0.045$; 7 S1 and 9 S2 sessions; one-tailed Wilcoxon rank sum test). Cyan shading and vertical dashed line as in **a**. (**l**) Same as in **k** for decoding choice. Performance was higher for S2 compared with S1 (79 ± 3% versus 72 ± 1% at 0.35 s; $U = 40$, $P = 0.021$; one-tailed Wilcoxon rank sum test). (**m**) Mean pairwise noise correlations between each responsive neuron and other responsive neurons (top), each DP neuron and other DP neurons (middle), or each SP neuron and other SP neurons (bottom). Noise correlations were higher in S2 (all $^{**}P < 5 \times 10^{-5}$; S1: 1,370 responsive, 536 SP and 338 DP neurons; S2: 607 responsive, 287 SP and 259 DP neurons; permutation tests).

the barrel column using intrinsic signal imaging (ISI; Online Methods). In S2, we also used the ISI response to estimate the center of the somatotopic representation of the stimulated whisker. In S1, both mean SP and mean DP (averaged across responsive and nonresponsive neurons) decreased with distance from the center of the barrel column (**Fig. 2i**). In S2, SP and DP both declined at most modestly with distances up to

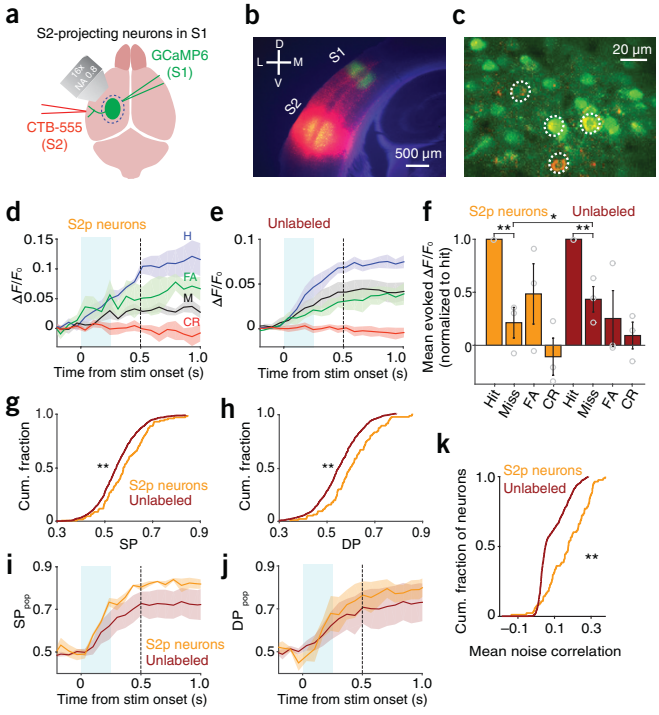

Figure 3 Feedforward propagation of activity from S1 to S2 predicts choice. (**a**) Schematic of retrograde labeling of S2p neurons in S1. (**b**) Coronal section showing CTB-Alexa555 (red) at the S2 injection site and GCaMP6 (green) in S1. (**c**) *In vivo* identification of S2p neurons. Dashed circles indicate GCaMP6-expressing neurons labeled with CTB-Alexa555. (**d**) Activity (mean ± s.e.m. $\Delta F/F_0$ across 3 mice, 8 sessions total) of S2p neurons averaged across trial types. Responses on hits were larger than on misses (0.040 ± 0.003 $\Delta F/F_0$ versus 0.020 ± 0.006 $\Delta F/F_0$; $t_{(87)} = 5.28$, $P = 9.24 \times 10^{-7}$; 88 neurons; paired *t*-test). Conventions as in **Figure 2a**. (**e**) Same as **d** for unlabeled neurons (hit: 0.027 ± 0.003 $\Delta F/F_0$; miss: 0.019 ± 0.007 $\Delta F/F_0$; $t_{(647)} = 13.19$, $P = 2.43 \times 10^{-35}$; 648 neurons; paired *t*-test). (**f**) Mean evoked $\Delta F/F_0$ responses normalized to hits across individual neurons (mean ± s.e.m. across mice; circles show individual mice). For both S2p and unlabeled neurons, responses on misses were smaller than on hits (miss/hit ratio: S2p: 0.21 ± 0.14; $z = 6.51$, $^{**}P = 7.43 \times 10^{-11}$; 88 neurons; unlabeled: 0.43 ± 0.12; $z = 13.81$, $^{**}P = 2.11 \times 10^{-43}$; 648 neurons; Wilcoxon sign rank tests), with slightly stronger modulation for S2p compared with unlabeled neurons ($^{*}P = 0.031$; permutation test). (**g**) S2p neurons showed higher SP compared with unlabeled neurons (medians: 0.57 versus 0.54; $^{**}P < 5 \times 10^{-5}$; 133 S2p and 1,134 unlabeled neurons; permutation test). Includes responsive and nonresponsive neurons. (**h**) S2p neurons showed higher DP than unlabeled neurons (medians: 0.58 versus 0.54; $^{**}P < 5 \times 10^{-5}$; permutation test). (**i**) Performance of a classifier (mean ± s.e.m. across mice) in decoding the stimulus condition from population activity reached a higher level for S2p compared with unlabeled neurons (73 ± 2% versus 63 ± 5% at 0.24 s after stimulus onset; $R = 34$, $P = 0.012$; 8 sessions; one-tailed Wilcoxon sign rank test). Conventions as in **Figure 2k**. (**j**) Same as **i** for decoding choice (68 ± 7% versus 62 ± 5% at 0.24 s; $R = 30$, $P = 0.055$; one-tailed Wilcoxon sign rank test). (**k**) Cumulative histograms of mean pairwise noise correlations between each S2p neuron and other S2p neurons (orange) or each unlabeled neuron and other unlabeled neurons (brown). Noise correlations were higher among S2p neurons ($^{**}P < 5 \times 10^{-5}$; 88 S2p and 648 unlabeled neurons; permutation test).

~400 µm from the center of the somatotopic representation (**Fig. 2j**). Thus, choice-related activity was clustered across somatosensory cortex, but clustering depended on cortical area.

Sensory and motor variables can be encoded not just by single neurons but also by activity patterns across neural populations. We quantified how well large populations of neurons in S1 and S2 encoded the whisker stimulus and the perceptual choice of the mouse using a machine learning classifier (Random Forests[31,32]; Online Methods). The classifier attempted to decode the stimulus condition (present versus absent) and the behavioral choice (lick versus no-lick) from the simultaneous activity of all responsive neurons, at each time point within a trial. Performance of the classifier in decoding the stimulus condition ('SP_{pop}') rose following stimulus onset for both S1 and S2, and reached higher levels in S1 than in S2 (**Fig. 2k**). Classifier performance in decoding the choice of the mouse ('DP_{pop}') rose following stimulus onset in both S1 and S2, but reached somewhat higher levels in S2 (**Fig. 2l**). Thus, decoding of tactile stimuli from population responses was better in S1, but decoding of choice was slightly better in S2.

Choice-related activity is thought to depend on trial-to-trial correlations in the responses of pairs of neurons[29,30] ('noise correlations'[33]; Online Methods). Consistent with stronger encoding of choice, S2 showed higher average noise correlations than S1 (0.19 ± 0.05 versus 0.09 ± 0.01; mean ± s.e.m. across mice; **Fig. 2m**). Stronger noise correlations in S2 were especially prominent in pairs of DP neurons (that is, pairs of neurons that both encoded choice; **Fig. 2m**).

To ensure that the differences in touch-related dynamics we observed between S1 and S2 were not due to differences among animals, we monitored S1 and S2 simultaneously in individual mice (11 sessions total from 4 mice; **Supplementary Fig. 3**; Online Methods). Responses on hits were larger than on misses in both S1 and S2 (**Supplementary Fig. 3e**). The miss/hit response ratio was smaller in S2 than in S1 (**Supplementary Fig. 3f**). The ratio of DP to SP for neurons in S2 was higher than for neurons in S1 (**Supplementary Fig. 3i**). At the population level, decoding of choice was slightly better in S2 than in S1 (**Supplementary Fig. 3k**). These results are consistent with S2 responses depending to a greater degree on choice.

Two results from simultaneous S1 and S2 imaging experiments suggest that perceptual detection may be associated with coordination of activity between S1 and S2. First, pairs of simultaneously recorded S1 and S2 neurons showed slightly higher noise correlations on hit than on miss trials (**Supplementary Fig. 3g,h**). Second, population decoding of choice was superior when using the pooled sets of S1 and S2 neurons, compared with decoding from either set alone (**Supplementary Fig. 3k**), implying that choice was encoded in at least a partly nonredundant manner across S1 and S2.

Feedforward propagation of task-related activity

To what degree can the strong encoding of choice in S2 be attributed to feedforward inputs from S1? To quantify feedforward propagation of activity from S1 to S2, we labeled S2-projecting (S2p) neurons in S1 using injections into S2 of cholera toxin subunit B, a retrograde tracer, conjugated to fluorescent dye[14–17,34] (**Fig. 3a,b**). We then identified these S2p neurons among the larger set of GCaMP6s-expressing neurons using *in vivo* imaging (8 sessions total from 3 mice; **Fig. 3c**). Unlabeled neurons presumably comprised both neurons that did not project to S2 and false-negative neurons that did project to S2 but were not labeled. Responses on hit trials were larger than on miss trials for both S2p neurons (hit – miss mean ± [95% CI]: 0.019 ± [0.005, 0.040] $\Delta F/F_0$; **Fig. 3d,f**) and unlabeled neurons (hit – miss mean ± [95% CI]: 0.010 ± [0.002, 0.017] $\Delta F/F_0$; **Fig. 3e,f**). However, S2p neurons showed slightly larger choice-related modulations (**Fig. 3f**; see also ref. 17).

Ideal observer analysis showed higher values of both SP (**Fig. 3g**) and DP (**Fig. 3h**) among S2p neurons than among unlabeled neurons. At the population-coding level, classifier performance in decoding the stimulus condition from S2p neurons reached a higher level compared

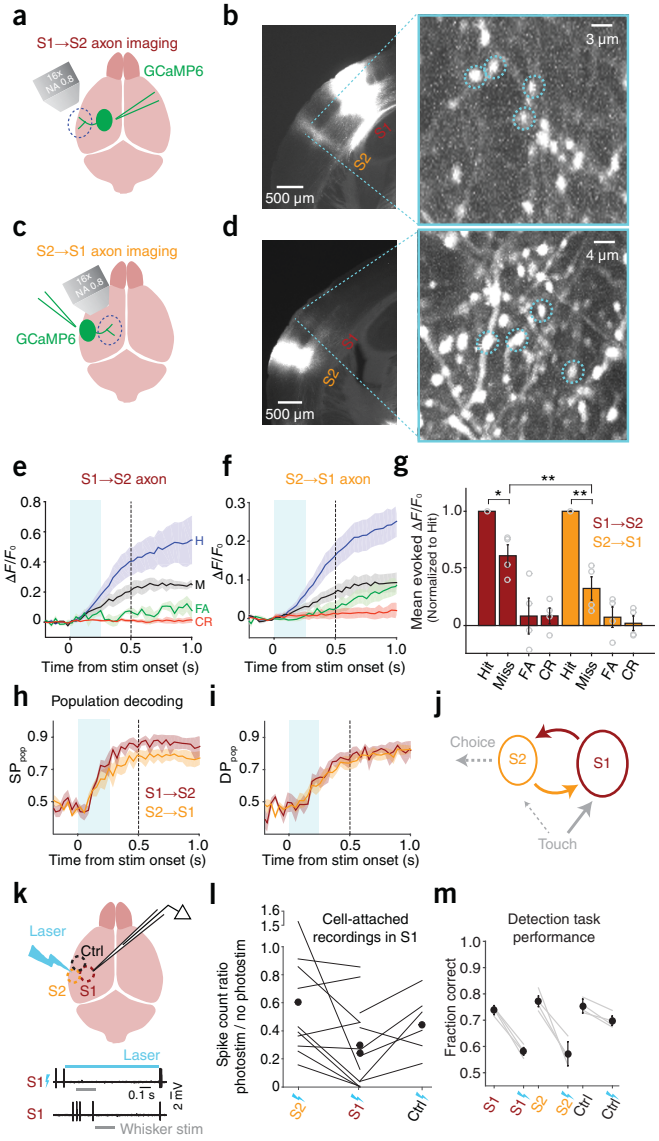

Figure 4 Activity in a feedback loop between S2 and S1. (**a**) Schematic of S1→S2 axon imaging experiment. AAV-GCaMP6 was injected in S1. A glass window was placed over S2. (**b**) Left, a coronal section showing GCaMP6 fluorescence in the injection (S1) and imaging (S2) areas. Right, example field of view from L2/3 of S2. Dashed circles indicate example regions of interest. (**c**) Schematic of S2→S1 axon imaging experiment. AAV-GCaMP6 was injected in S2. A glass window was placed over S1. (**d**) Left, a coronal section showing GCaMP6 fluorescence in the injection (S2) and imaging (S1) areas. Right, example field of view and regions of interest from L1 of S1. (**e**) Activity (mean ± s.e.m. $\Delta F/F_0$ across 4 mice, 7 sessions total, 160 axons total) of S1→S2 axons for each trial type. Responses on hits were larger than on misses (0.11 ± 0.027 $\Delta F/F_0$ versus 0.079 ± 0.029 $\Delta F/F_0$; $t_{(159)} = 3.25$, $P = 0.001$; 160 axons; paired *t*-test). Conventions as in **Figure 2a**. (**f**) Same as **e** for S2→S1 axons (10 sessions, 4 mice, 440 axons). Responses on hits were larger than on misses (0.031 ± 0.004 $\Delta F/F_0$ versus 0.016 ± 0.002 $\Delta F/F_0$; $t_{(439)} = 3.13$, $P = 0.002$; paired *t*-test). A subset of S2→S1 data in **f**,**g**–**i** are reanalyzed from ref. 38. (**g**) Mean evoked $\Delta F/F_0$ responses normalized to hits across individual axons (mean ± s.e.m. across mice; circles show individual mice). For both S1→S2 and S2→S1 axons, responses on misses were smaller than on hits (miss/hit ratio: S1→S2: 0.61 ± 0.10; $S = 99$, $^*P = 0.003$; 160 axons; S2→S1: 0.29 ± 0.11; $S = 313$, $^{**}P = 1.15 \times 10^{-18}$; 440 axons; sign tests), with stronger modulation for S2→S1 axons ($z = 3.82$, $^{**}P = 1.33 \times 10^{-4}$; Wilcoxon rank sum test). (**h**) Performance of a classifier (mean ± s.e.m. across mice) in decoding the stimulus condition from population activity reached a higher level for S1→S2 compared with S2→S1 axons (82 ± 2% versus 66 ± 6% at 0.28 s after stimulus onset; $z = 2.05$, $P = 0.044$; 7 S1→S2 and 10 S2→S1 sessions; one-tailed Wilcoxon rank sum test). Conventions as in **Figure 2k**. (**i**) Same as **h** for decoding choice. (**j**) Schematic of feedforward and feedback propagation of task-related activity (dashed: hypothetical functional pathways). (**k**) Top, optogenetic silencing experiment. In mice expressing channelrhodopsin-2 in GABAergic neurons, a 473-nm laser was directed over the C2 column (in S1), the whisker region of S2 or a control area (within S1 barrel cortex but ~1 mm from the C2 column). Photostimulation was randomly delivered on 30–40% of all behavioral trials. Bottom, example electrophysiology traces showing responses of an S1 neuron to whisker stimulation with and without laser illumination. (**l**) Cell-attached electrophysiology recordings were targeted to the C2 column in awake mice (16 neurons in 2 mice). The C2 whisker was stimulated in the presence or absence of laser illumination directed to the recording site (centered over the C2 column in S1), S2 or the control area. Silencing was quantified as the ratio of whisker-evoked spike count in the presence versus absence of illumination. S1 C2 area illumination produced stronger silencing of whisker-evoked responses than illumination of either S2 or the control area. Silencing was similar for S2 and the control area. Vertical axis is broken to accommodate one outlier. (**m**) Task performance (mean ± s.e.m. across 4 mice) was reduced by illuminating either S1 (from 74 ± 1.7% to 58 ± 1.5% correct) or S2 (from 77 ± 2.0% to 57 ± 4.6% correct), to a similar degree (S1 versus S2 reductions: $z = -0.81$, $P = 0.421$; 12 S1 and 15 S2 sessions; Wilcoxon rank sum test). Illuminating the control area caused a much smaller drop in performance (from 75 ± 2.6% to 70 ± 1.8% correct; S2 versus control area reductions: $z = -3.27$, $P = 0.001$; 12 control area sessions; Wilcoxon rank sum test). Gray lines, performance of individual mice averaged across sessions for interleaved trials with (bolts) and without (no bolts) illumination. Black symbols: mean ± s.e.m. across mice.

with unlabeled neurons (**Fig. 3i**). Classifier performance in decoding choice trended higher with S2p neurons than with unlabeled neurons (**Fig. 3j**). Moreover, noise correlations were stronger among pairs of S2p neurons than among pairs of unlabeled neurons (0.14 ± 0.04 versus 0.10 ± 0.02; mean ± s.e.m. across sessions; **Fig. 3k**). Thus, S2p neurons showed a more coordinated response and stronger association with perceptual choice.

A cortico-cortical loop for task-related activity

S1 and S2 are strongly and bidirectionally interconnected by long-range axonal projections[35–37]. Recurrent loops in cortical circuits can serve many computational functions, including amplifying and prolonging stimulus evoked activity[8,10]. To determine whether S1 and S2 could act in concert as a feedback loop during sensory decision making, we quantified stimulus- and choice-related activity propagating along feedforward (S1→S2) and feedback (S2→S1) axonal pathways (4 of 10 sessions of the S2→S1 data are from previously published experiments[38] and are reanalyzed here in greater detail). We expressed GCaMP6s in axons using adeno-associated virus (AAV) injections into either S1 (to monitor S1→S2 axons; **Fig. 4a**,**b**) or S2 (for S2→S1 axons[38]; **Fig. 4c**,**d**). We then imaged axonal activity during behavior[13] in S2 (S1→S2 axons, imaged in L2/3; **Fig. 4b**) or in S1 (S2→S1 axons[38], imaged in L1, a site of major top-down input to the dendrites of L2/3 neurons; **Fig. 4d** and **Supplementary Fig. 4**).

Axonal activity increased following stimulus onset, to higher levels on hits compared with misses in both S1→S2 axons (hit – miss mean ± [95% CI]: 0.029 ± [0.007, 0.054] $\Delta F/F_0$; **Fig. 4e**) and S2→S1 axons (hit – miss mean ± [95% CI]: 0.014 ± [0.005, 0.022] $\Delta F/F_0$; **Fig. 4f**). S2→S1 axons showed larger choice-related modulation compared with S1→S2 axons (**Fig. 4g**).

Performance of a classifier in decoding the stimulus condition from populations of axons rose following stimulus onset for both S1→S2 and S2→S1 axons, to a higher level for S1→S2 axons (**Fig. 4h**). Classifier performance in decoding choice also rose following stimulus onset, to

similar levels based on S1→S2 axons or S2→S1 axons (**Fig. 4i**). Thus, activity encoding both the sensory stimulus and the upcoming perceptual choice propagated along feedforward and feedback cortico-cortical axons between S1 and S2.

Our results are consistent with a model in which touch-evoked activity propagates in a feedback loop between S1 and S2 during formation of a perceptual choice, with 'readout' by downstream circuits occurring at least in part from S2 neurons (**Fig. 4j**). This model predicts that silencing S2 should impair task performance. However, S1 and S2 comprise densely interconnected networks[35–37], and the spatial resolution of cortical silencing is inherently too coarse to silence the two areas independently (for a description of the spatial resolution of cortical silencing, see ref. 39). Therefore, to test for a causal role of S2 in task performance, we devised a strategy based on comparing the behavioral impact of partially silencing S2 and S1 to different degrees.

We directed a laser to S1 (centered over the cortical column representing the C2 whisker, which was used to solve the task), to S2, or to a nearby control area (at stereotactic coordinates within the S1 barrel field but ~1 mm away from the C2 column) to optogenetically silence regions of cortex by photostimulation of GABAergic neurons expressing channelrhodopsin-2 (**Fig. 4k**)[39,40]. First, we recorded whisker-stimulus-evoked spikes from S1 neurons using loose-seal cell-attached recordings while directing the laser beam to S1, S2, or the control area. Silencing S2 or the control area led to decreases in S1 stimulus responses to 61% and 46% of baseline responses measured without photostimulation, respectively (**Fig. 4l**). Direct silencing of S1 by illumination of the recording site reduced responses further to 29% of baseline (**Fig. 4l**). Thus, direct silencing of somatosensory cortex yielded a 1.5-fold to 2-fold greater reduction in spiking than indirect silencing (via illumination of a nearby area).

Although silencing S2 or the control area reduced activity to similar levels in S1 (**Fig. 4l**), the behavioral impact of silencing S2 was markedly greater (**Fig. 4m** and **Supplementary Fig. 5**). In other words, task performance was more effectively disrupted by silencing S2 than by silencing a region of barrel cortex representing whiskers not used in the task, despite similar indirect effects on S1 activity. Moreover, direct silencing of either S2 or S1 decreased performance to similar levels (**Fig. 4m**). We conclude that the behavioral impact of reducing activity in either S1 or S2 was similar, indicating causal roles for both areas in tactile detection.

DISCUSSION

Our results show that as mice attempted to detect a faint whisker stimulus, larger responses within a cortico-cortical loop predicted perceptual choice (successful detection) on a trial-by-trial basis. Notably, 'late' stimulus responses in S1 have been linked to perceptual detection in both rodents[17,40] and primates[5]. These late responses occur at delays longer than the times for which feedforward activity can be sustained cell-autonomously by individual cortical neurons. We show here that touch-related activity propagates in specific pathways that form a direct loop between S1 and S2 (activity may also propagate between S1 and S2 indirectly[41]). Propagation in a loop can create circuit dynamics that act to amplify and sustain sensory activity[8], such as those of a Hebbian assembly. Although future work with electrophysiology will be required to define temporal dynamics, our work is consistent with the hypothesis that perception-related[5,17,40] late sensory responses in S1 reflect reverberation of activity[10] among cortical areas[42].

Overall, patterns of activity in S1 and S2 had obvious similarities and subtle but intriguing contrasts. In both S1 and S2, activity encoded the stimulus and the perceptual choice. Neurons in both S1 and S2 propagated stimulus- and choice-related activity to the other area. However, neurons in each area also showed key differences in their response properties (see also refs. 24,25). S2 activity was more associated with perceptual outcome than S1, whereas S1 activity better encoded the stimulus. While sensory stimuli are usually analog in nature, perception is often all-or-none. Neural representations of sensory stimuli must therefore converge into states representing discrete perceptions, perhaps via attractor dynamics. We found that trial-to-trial noise correlations (coordinated variability not explained by the stimulus) among pairs of S2 neurons were higher than among pairs of S1 neurons, consistent with a model in which S2 neurons encoded the binary perceptual outcome of each trial. Recent computational modeling has shown that top-down feedback of choice-related activity (similar to what we observed between S2 and S1) may be critical for the development of neuronal responses that reflect perceptual outcome[43].

Recently, a small number of studies[14–17,25,34,44] have examined *in vivo* responses of S1 neurons that project to S2 and have shown that these neurons have distinct intrinsic and task-related response properties. Here we found that L2/3 neurons that project from S1 to S2 tended to show higher choice-related activity[15,17] and stronger noise correlations than other L2/3 neurons. These characteristics were similar to those of L2/3 neurons located in S2, suggesting a partly feedforward inheritance of response properties[45,46] and even choice-related activity (compare ref. 47).

A limitation of our work is that we focused analysis of L2/3 neurons on the relatively small fractions in S1 (~37%) and S2 (~24%) that were task responsive (**Fig. 1h**). Studies across a wide variety of experimental contexts have revealed sparse activity patterns among cortical L2/3 neurons, but the nature of this sparseness remains poorly understood (reviewed in ref. 48). While we made no attempt to optimize our stimulus for the studied neurons, even systematic exploration of subthreshold whisker receptive fields has shown that activity is sparse among L2/3 neurons in S1 over the course of an experimental session[49]. The degree to which responses of L2/3 neurons change during learning of tactile tasks remains an active area of research[15,17,50]. Intriguingly, a recent study using a single-whisker tactile detection task found that detection-related activity emerged with learning specifically in S1 neurons that project to S2 (ref. 17).

We examined cortico-cortical dynamics during detection of passive touch in head-fixed animals, but S1–S2 interactions could depend on motor-sensory context. A recent study[24] used electrophysiology to quantify S1 and S2 spiking as rodents moved freely to interact with and identify textured surfaces. This study found that stimuli and choice were encoded via both the rate and timing of spikes across the S1–S2 network[24]. A second recent study[25] imaged activity in S1 and S2, including activity from neurons that project in each direction between these areas, and found behavior-dependent coordination of S1 and S2 activity during texture discrimination. Jointly with our data, these studies suggest that S1–S2 dynamics are critical to touch perception across multiple behavioral contexts. Together, our results suggest that the transformation from raw sensory input to perception occurs via feedforward computations that are reinforced through feedback in a cortico-cortical loop.

METHODS

Methods, including statements of data availability and any associated accession codes and references, are available in the online version of the paper.

Note: Any Supplementary Information and Source Data files are available in the online version of the paper.

ACKNOWLEDGMENTS

We thank V. Jayaraman, R. Kerr, D. Kim, L. Looger, K. Svoboda and the HHMI Janelia Farm GENIE Project for GCaMP6. We thank S. Peron for MATLAB

software, T. Shelley for instrument fabrication, and K. Severson and E. Finkel for mouse husbandry. We thank E. Finkel, D. Xu, K. Severson, B. Bari, M. Chevee, K. Svoboda, S. Brown, J. Cohen and S. Mysore for comments on the manuscript. This work was supported by the Whitehall Foundation, Klingenstein Fund, the Johns Hopkins Science of Learning Institute, NIH grant R01NS089652 (D.H.O.) and NIH core grant P30NS050274. G.M. was supported by a JSPS Postdoctoral Fellowship for Research Abroad.

AUTHOR CONTRIBUTIONS

S.E.K. and D.H.O. planned the project. S.E.K. performed imaging, behavioral, and optogenetics experiments. H.Y. performed electrophysiology and optogenetics experiments. S.E.K. and D.H.O. analyzed data. G.M. established S2 targeting methods. S.E.K. and D.H.O. wrote the paper with comments from H.Y. and G.M.

COMPETING FINANCIAL INTERESTS

The authors declare no competing financial interests.

1. de Lafuente, V. & Romo, R. Neural correlate of subjective sensory experience gradually builds up across cortical areas. *Proc. Natl. Acad. Sci. USA* **103**, 14266–14271 (2006).
2. Felleman, D.J. & Van Essen, D.C. Distributed hierarchical processing in the primate cerebral cortex. *Cereb. Cortex* **1**, 1–47 (1991).
3. Gilbert, C.D. & Li, W. Top-down influences on visual processing. *Nat. Rev. Neurosci.* **14**, 350–363 (2013).
4. Bastos, A.M. *et al.* Canonical microcircuits for predictive coding. *Neuron* **76**, 695–711 (2012).
5. Cauller, L. Layer I of primary sensory neocortex: where top-down converges upon bottom-up. *Behav. Brain Res.* **71**, 163–170 (1995).
6. Hopfield, J.J. Neural networks and physical systems with emergent collective computational abilities. *Proc. Natl. Acad. Sci. USA* **79**, 2554–2558 (1982).
7. Douglas, R.J., Koch, C., Mahowald, M., Martin, K.A. & Suarez, H.H. Recurrent excitation in neocortical circuits. *Science* **269**, 981–985 (1995).
8. Seung, H.S. in *The Handbook of Brain Theory and Neural Networks* 94–97 (MIT Press, 2003).
9. Murphy, B.K. & Miller, K.D. Balanced amplification: a new mechanism of selective amplification of neural activity patterns. *Neuron* **61**, 635–648 (2009).
10. Wang, X.J. Probabilistic decision making by slow reverberation in cortical circuits. *Neuron* **36**, 955–968 (2002).
11. Douglas, R.J. & Martin, K.A. Opening the grey box. *Trends Neurosci.* **14**, 286–293 (1991).
12. Glickfeld, L.L., Andermann, M.L., Bonin, V. & Reid, R.C. Cortico-cortical projections in mouse visual cortex are functionally target specific. *Nat. Neurosci.* **16**, 219–226 (2013).
13. Petreanu, L. *et al.* Activity in motor-sensory projections reveals distributed coding in somatosensation. *Nature* **489**, 299–303 (2012).
14. Chen, J.L., Carta, S., Soldado-Magraner, J., Schneider, B.L. & Helmchen, F. Behaviour-dependent recruitment of long-range projection neurons in somatosensory cortex. *Nature* **499**, 336–340 (2013).
15. Chen, J.L. *et al.* Pathway-specific reorganization of projection neurons in somatosensory cortex during learning. *Nat. Neurosci.* **18**, 1101–1108 (2015).
16. Yamashita, T. *et al.* Membrane potential dynamics of neocortical projection neurons driving target-specific signals. *Neuron* **80**, 1477–1490 (2013).
17. Yamashita, T. & Petersen, C.Ch. Target-specific membrane potential dynamics of neocortical projection neurons during goal-directed behavior. *Elife* **5**, e15798 (2016).
18. Makino, H. & Komiyama, T. Learning enhances the relative impact of top-down processing in the visual cortex. *Nat. Neurosci.* **18**, 1116–1122 (2015).
19. Suter, B.A. & Shepherd, G.M. Reciprocal interareal connections to corticospinal neurons in mouse M1 and S2. *J. Neurosci.* **35**, 2959–2974 (2015).
20. Carvell, G.E. & Simons, D.J. Thalamic and corticocortical connections of the second somatic sensory area of the mouse. *J. Comp. Neurol.* **265**, 409–427 (1987).
21. Carvell, G.E. & Simons, D.J. Somatotopic organization of the second somatosensory area (SII) in the cerebral cortex of the mouse. *Somatosens. Res.* **3**, 213–237 (1986).
22. Kleinfeld, D. & Delaney, K.R. Distributed representation of vibrissa movement in the upper layers of somatosensory cortex revealed with voltage-sensitive dyes. *J. Comp. Neurol.* **375**, 89–108 (1996).
23. Kwegyir-Afful, E.E. & Keller, A. Response properties of whisker-related neurons in rat second somatosensory cortex. *J. Neurophysiol.* **92**, 2083–2092 (2004).
24. Zuo, Y. *et al.* Complementary contributions of spike timing and spike rate to perceptual decisions in rat S1 and S2 cortex. *Curr. Biol.* **25**, 357–363 (2015).
25. Chen, J.L., Voigt, F.F., Javadzadeh, M., Krueppel, R. & Helmchen, F. Long-range population dynamics of anatomically defined neocortical networks. *Elife* **5**, e14679 (2016).
26. Chen, T.W. *et al.* Ultrasensitive fluorescent proteins for imaging neuronal activity. *Nature* **499**, 295–300 (2013).
27. Britten, K.H., Newsome, W.T., Shadlen, M.N., Celebrini, S. & Movshon, J.A. A relationship between behavioral choice and the visual responses of neurons in macaque MT. *Vis. Neurosci.* **13**, 87–100 (1996).
28. Parker, A.J. & Newsome, W.T. Sense and the single neuron: probing the physiology of perception. *Annu. Rev. Neurosci.* **21**, 227–277 (1998).
29. Nienborg, H., Cohen, M.R. & Cumming, B.G. Decision-related activity in sensory neurons: correlations among neurons and with behavior. *Annu. Rev. Neurosci.* **35**, 463–483 (2012).
30. Shadlen, M.N., Britten, K.H., Newsome, W.T. & Movshon, J.A. A computational analysis of the relationship between neuronal and behavioral responses to visual motion. *J. Neurosci.* **16**, 1486–1510 (1996).
31. Hastie, T., Tibshirani, R. & Friedman, J.H. *The Elements of Statistical Learning: Data Mining, Inference, and Prediction* 2nd edn. (Springer, 2009).
32. Huber, D. *et al.* Multiple dynamic representations in the motor cortex during sensorimotor learning. *Nature* **484**, 473–478 (2012).
33. Cohen, M.R. & Kohn, A. Measuring and interpreting neuronal correlations. *Nat. Neurosci.* **14**, 811–819 (2011).
34. Clancy, K.B., Schnepel, P., Rao, A.T. & Feldman, D.E. Structure of a single whisker representation in layer 2 of mouse somatosensory cortex. *J. Neurosci.* **35**, 3946–3958 (2015).
35. Aronoff, R. *et al.* Long-range connectivity of mouse primary somatosensory barrel cortex. *Eur. J. Neurosci.* **31**, 2221–2233 (2010).
36. Cauller, L.J., Clancy, B. & Connors, B.W. Backward cortical projections to primary somatosensory cortex in rats extend long horizontal axons in layer I. *J. Comp. Neurol.* **390**, 297–310 (1998).
37. Mao, T. *et al.* Long-range neuronal circuits underlying the interaction between sensory and motor cortex. *Neuron* **72**, 111–123 (2011).
38. Yang, H., Kwon, S.E., Severson, K.S. & O'Connor, D.H. Origins of choice-related activity in mouse somatosensory cortex. *Nat. Neurosci.* **19**, 127–134 (2016).
39. Guo, Z.V. *et al.* Flow of cortical activity underlying a tactile decision in mice. *Neuron* **81**, 179–194 (2014).
40. Sachidhanandam, S., Sreenivasan, V., Kyriakatos, A., Kremer, Y. & Petersen, C.C. Membrane potential correlates of sensory perception in mouse barrel cortex. *Nat. Neurosci.* **16**, 1671–1677 (2013).
41. Theyel, B.B., Llano, D.A. & Sherman, S.M. The corticothalamocortical circuit drives higher-order cortex in the mouse. *Nat. Neurosci.* **13**, 84–88 (2010).
42. Manita, S. *et al.* A top-down cortical circuit for accurate sensory perception. *Neuron* **86**, 1304–1316 (2015).
43. Engel, T.A., Chaisangmongkon, W., Freedman, D.J. & Wang, X.J. Choice-correlated activity fluctuations underlie learning of neuronal category representation. *Nat. Commun.* **6**, 6454 (2015).
44. Sato, T.R. & Svoboda, K. The functional properties of barrel cortex neurons projecting to the primary motor cortex. *J. Neurosci.* **30**, 4256–4260 (2010).
45. El-Shamayleh, Y., Kumbhani, R.D., Dhruv, N.T. & Movshon, J.A. Visual response properties of V1 neurons projecting to V2 in macaque. *J. Neurosci.* **33**, 16594–16605 (2013).
46. Movshon, J.A. & Newsome, W.T. Visual response properties of striate cortical neurons projecting to area MT in macaque monkeys. *J. Neurosci.* **16**, 7733–7741 (1996).
47. Smolyanskaya, A., Haefner, R.M., Lomber, S.G. & Born, R.T. A modality-specific feedforward component of choice-related activity in MT. *Neuron* **87**, 208–219 (2015).
48. Barth, A.L. & Poulet, J.F. Experimental evidence for sparse firing in the neocortex. *Trends Neurosci.* **35**, 345–355 (2012).
49. Ramirez, A. *et al.* Spatiotemporal receptive fields of barrel cortex revealed by reverse correlation of synaptic input. *Nat. Neurosci.* **17**, 866–875 (2014).
50. Peron, S.P., Freeman, J., Iyer, V., Guo, C. & Svoboda, K. A cellular resolution map of barrel cortex activity during tactile behavior. *Neuron* **86**, 783–799 (2015).

Editorial Summary

Feedforward and feedback synaptic pathways shape how neural activity evolves across cortical areas, but they are difficult to monitor using traditional methods during behavior. The authors use pathway-specific and cellular-resolution *in vivo* imaging to quantify sensory and decision-related neural activity both within and propagating between two cortical areas critical for touch perception.

ONLINE METHODS

Mice. All procedures were in accordance with protocols approved by the Johns Hopkins University Animal Care and Use Committee. We report calcium imaging experiments from 16 male C57BL/6NHsd (Harlan) mice and from 2 male and 2 female C57BL/6J Thy1-GCaMP6s GP4.3 (Jackson Labs) mice[51], with ages ranging from 9 to 16 weeks. We report optogenetic silencing experiments from 4 females and 1 male obtained by crossing PV-IRES-Cre (Jackson Labs: 008069; B6;129P2-*Pvalb*$^{tm1(cre)Arbr}$/J)[52] with Ai32 (Jackson Labs: 012569; B6;129S-*Gt(ROSA)26Sor*$^{tm32(CAG-COP4*H134R/EYFP)Hze}$/J)[53] mice on a mixed background, with ages ranging from 10 to 12 weeks. Mice were housed in a vivarium with reverse light-dark cycle (12 h each phase). Experiments occurred during the dark phase. Mice were housed in groups of up to five before the start of water restriction, after which mice were housed singly. Assignments of mice to experimental conditions and analyses are detailed in **Supplementary Figure 6**.

Intrinsic signal imaging. After recovery from headpost surgery (>24 h) or headpost surgery plus GCaMP6 injection and cranial window implantation (7–9 d), mice were lightly anesthetized with isoflurane (0.5–1%) and chlorprothixene (0.02 ml of 0.36 mg ml^{-1}, intramuscular). Intrinsic signal imaging (ISI) was performed as described[54]. In all virus-injected mice, the target whisker was right C2. ISI was performed through the cranial window or a clear skull cap[39]. Whisker S2 could be identified as a region of decreased reflectance clearly delineated from whisker S1. Sound from the piezo stimulator is a potential source of response during ISI mapping of regions in the vicinity of S2. As a control experiment to distinguish auditory responses from tactile responses, ISI was occasionally performed without threading the target whisker into the stimulator, which otherwise remained in a nearly identical position. Areas responsive under this condition were considered auditory areas and were distinct from whisker S2. In Thy1-GCaMP6s mice used for simultaneous S1 and S2 imaging, responses to several different whiskers (right B2, B3, C2, C3) were mapped through the cranial window after recovery from surgery. We selected a target whisker for behavioral training on the basis of the criterion that the target whisker's responsive regions in both S1 and S2 could be covered by the same two-photon field of view. As a result, the B3 whisker was used in 2 mice, B2 in 1 mouse, and C3 in 1 mouse. We further validated S1 and S2 identification using wide-field fluorescence imaging under the same field of view used for ISI. Taking advantage of homogeneous expression of GCaMP6s across cortex, we identified regions showing evoked fluorescence in response to the same whisker stimulation protocol used for ISI. In all cases, wide-field imaging yielded two clearly separated regions (corresponding to S1 and S2) that matched those identified by ISI.

Behavioral task. Mice were trained to perform a tactile detection task while head-fixed. Behavioral apparatus was controlled by BControl software (C. Brody, Princeton University). For 7–10 d before training, mice received 1 ml d^{-1} of water. On training days, mice were weighed before and after each training session to determine water consumed. Mice were allowed to perform the task until sated. Additional water was given if mice consumed <0.3 ml. In the first 1–2 sessions, mice received a drop of water (~6 µl) each time the tongue contacted a 'lick port' tube placed near their snouts. In subsequent sessions, mice were operantly conditioned to lick at the lick port in response to a passive whisker deflection. All whiskers except the target whisker were trimmed to near the base. The target whisker was threaded into a glass pipette attached to a piezo actuator (Piezo Systems), with ~3–5 mm at the base exposed. For training, on Go trials, the whisker was deflected for 0.5 s with a 20 Hz sinusoidal deflection (rostral to caudal, peak angular speed ~800 deg s^{-1}). A hit trial occurred when mice licked the lick port within a response window, and a drop of water was delivered (~6 µl). The response window was defined as 0.2–2 s after onset of whisker stimulation. The initial 0.2 s after stimulus onset was a 'grace period' in which licks had no consequence. On Go trials, if mice did not lick within the 1.8 s response window, it was scored as a miss trial, and no reward or punishment was delivered. Go trials were randomly mixed with NoGo trials, in which the whisker was not deflected. No more than 3 consecutive trials of the same type were allowed. On NoGo trials, if mice licked within the response window, it was scored as a false alarm, and mice were punished with a 3–5 s timeout. If mice licked during the timeout, an additional timeout was triggered. A correct rejection occurred when mice withheld licking during the response window. Correct rejections were not rewarded. After performance reached >65% correct, a 0.1-s auditory cue (8 kHz tone, ~80 dB SPL) was introduced starting 1 s before stimulus onset. During all sessions, ambient white noise (cut off at 40 kHz, ~80 dB SPL) was played through a separate speaker to mask any other potential auditory cues associated with movement of the piezo stimulator. Mice were considered trained when performance reached >70% correct for at least 2 consecutive days. Typically, mice were trained one session per day for 7–10 d to reach this criterion. Trials with premature licks occurring close to stimulus onset (–0.51 s to +0.12 s) were excluded from subsequent analysis. Only 2% of trials had reaction times occurring after the end of this premature lick window but before the end of the grace period. There was a modest trend toward higher pre-stimulus $\Delta F/F_0$ on miss trials in S1 (**Supplementary Fig. 7**), which could be due to occasional pre-stimulus whisker motion. We considered the possibility that self-generated whisker or tongue movements early in the trial could partly account for the different responses we observed in hit versus miss trials. We used high-speed video to monitor whisker and tongue motion and thereby to obtain a set of trials in which we could confirm negligible motion (**Supplementary Fig. 8**). We observed a robust hit versus miss difference in evoked $\Delta F/F_0$ for this subset of trials (**Supplementary Fig. 8**).

Two-photon calcium imaging of layer 2/3 somata. A circular craniotomy was made over the left barrel cortex (2.5 mm diameter; center relative to bregma: lateral, 3.5 mm; caudal, 1.3 mm) of P40–50 mice. The dura was left intact. GCaMP6s or, in the case of one animal used in S1 cell body calcium imaging[26], GCaMP6f, was expressed under the human synapsin-1 (*SYN1*) promoter following infection with recombinant adeno-associated virus (serotype 2/1, Syn.GCaMP6s.WPRE.SV40, or Syn.GCaMP6f.WPRE.SV40, University of Pennsylvania Gene Therapy Program Vector Core). Injections were made at 4–6 sites within the craniotomy (30–50 nl per site; depth, 250–300 µm; rate, ~1 nl s^{-1}) using a glass pipette (30–50 µm diameter). After virus injection, the craniotomy was covered with an imaging window made by gluing together two pieces of microscope cover glass[32]. The smaller piece (Fisher; number 2 thickness) was fitted into the craniotomy and the larger piece (number 1.5 thickness) was glued to the bone surrounding the craniotomy[32]. Intrinsic signal imaging was used to localize a barrel column or whisker S2 within the area of the cranial window (7–9 d after window implantation). All whiskers on the right side of the snout except the relevant one (a row C whisker, except as noted below for simultaneous S1 and S2 imaging) were trimmed after the intrinsic signal imaging. Mice were then water restricted for 2 weeks before training. Imaging was started 3–5 weeks after surgery.

For simultaneous imaging of S1 and S2, Thy1-GCaMP6s mice were prepared using the same method as described above except that a row B whisker (B2 or B3) was used for 3 of 4 mice and C3 whisker for 1 mouse. S1 and S2 were identified using intrinsic signal imaging and wide-field imaging of evoked GCaMP6s fluorescence as described above.

Images were acquired on a custom two-photon microscope (http://openwiki.janelia.org/wiki/display/shareddesigns/MIMMS) equipped with a resonant scanning module (Thorlabs), GaAsP photomultiplier tubes (Hamamatsu) and a 16× 0.8 NA microscope objective (Nikon). GCaMP6 was excited at 1,000 nm (40–60 mW at specimen) with a Ti:sapphire laser (Chameleon Ultra II, Coherent). Imaging fields were restricted to areas where GCaMP6 expression overlapped with the desired barrel columns or the identified whisker area of S2. For S2 imaging sessions, we rotated mice ≤ 5 degrees from the sagittal plane to enable access of the microscope objective to the cranial window. Mice exhibited no signs of discomfort. We did not rotate mice for simultaneous imaging of S1 and S2 sessions because the imaged whisker representation in S2 was located relatively medially. The field of view ranged from 760 µm × 790 µm to 440 µm × 485 µm (440 × 512 pixels; pixel size, 1.72 µm × 1.55 µm to 1.0 µm × 0.94 µm). Images were acquired continuously at 30 Hz using ScanImage[55] 4.2 (http://www.scanimage.org/). A movie, corresponding to a single trial, consisted of 140 image frames. In 2 sessions from 1 mouse, images were acquired at 15 Hz and movies comprised 65 frames.

Retrograde labeling of S2-projecting neurons in S1. A subset of mice that were used for S1 soma imaging experiments were injected *post hoc* with a retrograde tracer, CTB-Alexa555 (5 µg µl^{-1} in PBS, Invitrogen), in S2 localized by intrinsic signal imaging. The *post hoc* injection occurred shortly after conclusion of behavioral experiments. A small hole was drilled through the

glass cranial window. One hundred nanoliters of CTB-Alexa555 was injected (depth, 400–500 µm; rate, ~1 nl s^{-1}) through the hole via a glass pipette (30–50 µm). The injection site was sealed with dental cement. Seven to 10 d after the injection, the labeled cells were examined under the two-photon microscope. To localize co-labeling, GCaMP6-labeled cells and CTB-Alexa555-labeled cells were excited at 940 nm or 1,020 nm, respectively (40–60 mW at specimen). Fluorescence emission was separated using a 568-nm dichroic (FF568-Di01-35.5x50.2, Semrock), passed through green (ET525/70m-2p, Chroma) and red (FF01-625/90-30-D, Semrock) channel filters before detection with two GaAsP photomultiplier tubes (Hamamatsu).

Two-photon calcium imaging of axons. A subset of data for S2→S1 axons (4 of 10 sessions) comes from published experiments[38] and is analyzed here in greater detail. Adeno-associated virus (serotype 2/1, Syn.GCaMP6s.WPRE.SV40) was injected into the C2 barrel column (identified by ISI) for S1→S2 axon imaging or whisker S2 area (relative to bregma: lateral, 4.3 mm; caudal, 1 mm) for S2→S1 axon imaging at two depths (250 µm and 350 µm; 30–40 nl each; ~1 nl s^{-1}) and the site was covered with a cranial window. For S2→S1 axon imaging, intrinsic signal imaging was performed through the window. GCaMP6s expression was examined under a wide-field fluorescence microscope, and mice showing excessive cell body fluorescence outside the ISI-localized S2 region were not used for experiments. Imaging planes were from layer 2/3 of S2 (150–250 µm from pial surface) for S1→S2 axon imaging or layer 1 of S1 (70–100 µm from pial surface) for S2→S1 axon imaging. The field of view was 100 µm × 108 µm (440 × 512 pixels; pixel size, 0.23 µ× 0.21 µm). Images were acquired continuously at 30 Hz using ScanImage 4.2. A movie, corresponding to a single trial, consisted of 140 image frames.

Optogenetic silencing. PV-IRES-Cre;Ai32 mice were implanted with a clear skull cap[39], or a coverglass over the left barrel cortex following a circular craniotomy. Light from a 473-nm laser (MBL-III-473-100, Ultralasers) was passed through an acousto-optic modulator (MTS110-A3-VIS, QuantaTech), focused into a multimode optical fiber, recollimated, and directed onto the targeted cortical area. The beam at the skull or cranial window had an approximately Gaussian profile with FWHM of 600 µm. Photostimulation was randomly delivered on 30–40% of all trials. Photostimulation comprised a train of 5 ms pulses at 100 Hz delivered from −300 ms to +2,200 ms relative to the time of whisker stimulus onset for Go trials. The same time window was used for NoGo trials. Average power at the brain surface was ~3 mW for glass-implanted animals ($n = 2$) or ~7 mW for those with a clear skull cap[39] ($n = 2$). A visual masking flash (2 ms pulses at 10 Hz) was delivered for the duration of every trial via a 470-nm LED (7007-PB000-D, LEDdynamics) placed near the eyes. For behavioral experiments, the laser was steered over the C2 column in S1 (localized with ISI), whisker S2, or a control area in separate sessions within the same animal. The control area was separated from the C2 column and S2 illumination sites by ~1 mm, but at stereotactic coordinates still within whisker S1 (4 mm lateral, 0.3 mm caudal to bregma). Cell-attached recordings for electrophysiological calibration were performed as described previously[56]. One of the two mice used for recordings was previously used for the behavioral silencing experiments. The illumination site for S1 electrophysiological recordings (either S1 versus S2, or S1 versus control area) was varied every ~50 sweeps with the starting site varied across neurons. The C2 area of S1 was accessed by the recording pipette through a hole drilled in a previously implanted cranial window. Loose-seal cell-attached recordings were made in awake mice while the C2 whisker was stimulated in the presence or absence of 473-nm laser pulses to the recording site (S1, C2 area), S2 or the control area (S1, non-C2).

Two-photon calcium imaging of layer 2/3 somata: data analysis. A line-by-line correction algorithm was used to correct for brain motion[32,50]. For each behavioral trial, we used five consecutive frames with a minimum of luminance changes to generate an average reference image. Each line was registered to the reference image by maximizing the line-by-line Pearson correlation. Regions of interest (ROIs) corresponding to individual neurons were manually selected with the help of maximum intensity and s.d. projections across movie frames. For each ROI, the time series of raw fluorescence was estimated by averaging all pixels within the ROI. Neuropil signal surrounding each ROI was estimated by averaging all pixels, excluding those from neighboring ROIs, within a 2-pixel-wide ring that started 2 pixels away from the border of the ROI. This neuropil signal was subtracted from the raw fluorescence time series to yield the corrected fluorescence time series[26,57]: $F(t) = F_{raw}(t) - r \times F_{neuropil}(t)$, with $r = 0.3$. $\Delta F/F_0$ was calculated as $(F–F_0)/F_0$, where F_0 was the mean F over 8 baseline frames immediately preceding the stimulus onset time for each trial. Evoked $\Delta F/F_0$ was calculated as the mean $\Delta F/F_0$ over 5 frames following the stimulus onset time and before the answer lick (frames 56–60 with stimulus onset between frames 52 and 53; results were similar for later 5-frame windows; **Supplementary Fig. 9**). For one mouse imaged at 15 Hz, F_0 was the mean F over 4 baseline frames immediately preceding the stimulus onset time, and evoked $\Delta F/F_0$ was the mean $\Delta F/F_0$ over 3 frames following the stimulus onset time (frames 28–30 with stimulus onset between frames 26 and 27).

To assign each neuron as 'responsive' or 'nonresponsive', evoked $\Delta F/F_0$ was calculated as above, except using the 20 frames (10 frames for 15 Hz imaging) immediately following stimulus onset for the post-stimulus window. For each neuron, a Wilcoxon signed rank test (for samples with absolute value skew <0.6) or a sign test (absolute value skew >0.6) was performed on the evoked $\Delta F/F_0$ values. If the resulting P-value was <0.01, the neuron was considered responsive; otherwise it was nonresponsive.

Two-photon calcium imaging of axons: data analysis. Analysis procedures were as described above except that neuropil subtraction was not implemented. To distinguish ROIs that belong to the same axon from those that belong to different axons, we used a correlation-based method (adapted from ref. 13) to build clusters of highly correlated ROIs (**Supplementary Fig. 4**). Briefly, varicosities that were clearly part of the same axon were identified by visual inspection (8 sessions). Correlation coefficients of these varicosities were calculated from $\Delta F/F_0$ concatenated from trials over an entire session and were compared to all pairwise correlation coefficients. $\Delta F/F_0$ was calculated as $(F - F_0)/F_0$, where F_0 was the 15th percentile of F. Correlation coefficients of varicosities from the same axon were clearly distinct from the rest and showed values larger than 0.7 on average. We selected all sets of two varicosities with correlation coefficient >0.7. These N pairs of varicosities were randomly ordered into a N-tuple, $P = (P_1,P_2,\ldots,P_i,\ldots P_N)$. We began an iterative clustering process by initializing N clusters, $C = (C_1,C_2,\ldots,C_i,\ldots C_N)$, where the ith cluster C_i contained the two varicosities from P_i. Next, P_2 was tested for inclusion in C_1. If $P_2 \cap C_1 \neq \{\}$, then the elements of P_2 were added to C_1. P_3 was then tested for inclusion in C_1 and C_2, and so on. That is, for all $j < i$, the elements of P_i were added to C_j if $P_i \cap C_j \neq \{\}$. At the end of this process, C contained overlapping clusters. Finally, we reduced each cluster to its unique elements and selected for subsequent analysis only those clusters having no overlap with previous clusters. That is, C_i was selected if and only if $C_i \cap C_j = \{\}$ for all $j < i$. For subsequent analysis, $\Delta F/F_0$ was calculated as $(F - F_0)/F_0$, where F_0 was the mean F over 8 baseline frames immediately preceding the time of possible stimulus onset on each trial. The $\Delta F/F_0$ for each putative axon was calculated as the mean $\Delta F/F_0$ from all responsive varicosities within a cluster.

Single-neuron ideal observer analysis. We used receiver operating characteristic (ROC) analysis to calculate the detect probability (identical to "choice probability"[27]) and stimulus probability. A decision variable (DV) was assigned for each trial on the basis of the neural response. DV was the evoked $\Delta F/F_0$ as defined above. Trials were grouped by the mouse's choice (lick versus no-lick, for detect probability) or by stimulus condition (present versus absent, for stimulus probability). An ROC curve was obtained by systematically varying the criterion value across the full range of DV (using MATLAB "perfcurve"). The area under the ROC curve (AUC) represents the performance of an ideal observer in categorizing trials based on the DV. Detect probability was the AUC for discriminating choice. Stimulus probability was the AUC for discriminating the stimulus condition. A 95% confidence interval for each AUC was obtained by bootstrap (MATLAB "perfcurve").

Noise correlation analysis. Noise correlations[33] were quantified as Pearson's correlation coefficient between evoked $\Delta F/F_0$ values for a pair of neurons across all Go trials. The values were averaged across all pairs to obtain the mean noise correlation for a neuron.

Population decoding analysis. We used Random Forests ensemble classifiers[31] (via MATLAB "TreeBagger" class with 300 trees and minimum leaf size of 1) to discriminate the stimulus condition (Go trials versus NoGo trials) or choice (hits and false alarms versus misses and correct rejections) on the basis of the vector of $\Delta F/F_0$ for all responsive neurons at a given time point (image frame) during the

trial. A separate classifier was trained on each time point. Classifier performance was quantified as the area under the ROC curve for classification of out-of-bag observations. We denote the performance in decoding the stimulus condition based on population responses as SP_{pop}, by analogy to our ideal observer 'stimulus probability' quantity for single neurons. Similarly, we denote performance on decoding choice as DP_{pop}. In **Figure 3**, data from 1 mouse were acquired at 15 Hz whereas data from 2 mice were acquired at 30 Hz. We accommodated the slower imaging speed for this 1 mouse as follows. For display in **Figure 3d**,**e**, we combined 15 Hz and 30 Hz movies by excluding every other frame of the 30 Hz movies. Random Forest classification was performed using all frames (65 frames for 15 Hz, 140 frames for 30 Hz). For **Figure 3i**,**j**, decoding performance curves were combined across different imaging speeds by excluding every other frame of the 30 Hz movies. The image frame at which decoder performance diverged was defined as the first frame at which a one-tailed Wilcoxon rank sum test (**Figs. 2k**,**l** and **4h**,**i**) or a one-tailed Wilcoxon sign rank test (**Fig. 3i**,**j** and **Supplementary Fig. 3j**,**k**) reached $P < 0.05$. Statistical tests for population decoders were one-tailed and performed across sessions rather than mice because (i) each analysis began with a hypothesis for the sign of any difference, and (ii) each behavioral session yielded one decoder performance curve.

Data analysis: pooling across sessions and mice. Our convention in the text and figures is to report variability across mice. Unless otherwise noted, we used two strategies to combine data from multiple behavioral sessions for an individual mouse. For cumulative histograms in **Figure 2d**, we pooled ROIs across sessions to obtain histograms for each mouse, and then averaged these histograms. For mean $\Delta F/F_0$ time series in **Figures 2a**,**b**, **3d**,**e** and **4e**,**f**, bar graphs and scatter plots in **Figures 1h**, **2c**, **3f** and **4g**, plots of SP or DP versus distance in **Figure 2i**,**j**, and population decoder time series in **Figures 2k**,**l**, **3i**,**j** and **4h**,**i**, we averaged values across sessions for each mouse. Cumulative histograms in **Figures 2g**,**h**,**m** and **3g**,**h**,**k** were obtained by pooling all data across mice and sessions. The number of monitored or responsive neurons could vary from session to session for a given mouse. For brevity in the text and figure legends, therefore, we report the number of neurons obtained on average across sessions for each mouse. We also report the total number of neurons or observations used for each statistical test.

Statistics. We report data as mean ± s.e.m. unless otherwise noted. Statistical tests were two-tailed except where noted. We made no adjustments for multiple comparisons. We chose statistical tests in the following order of decreasing preference: (i) parametric tests when appropriate (paired and unpaired *t*-tests); (ii) rank- and sign-based nonparametric tests (Wilcoxon signed rank, Wilcoxon rank sum, sign test); Kolmogorov-Smirnov tests; (iii) randomization tests (permutation and bootstrap). Prior to using *t*-tests, we assessed normality using quantile–quantile plots. Prior to using Wilcoxon signed rank tests, we confirmed symmetry of the tested sample about its median (defined as absolute value skewness < 0.6); otherwise we used a sign test.

To test whether the median pairwise distance (**Fig. 2g**) among SP neurons, D_{SP}, was the same as the median distance among all neurons, D_{all}, we used a bootstrap method. The test statistic was the observed difference in median distances, $Y = D_{all} - D_{SP}$. A bootstrap replicate, Y^*, was obtained from each of 20,000 bootstrap samples. Each replicate was calculated as the difference between D_{all} and the median of N_{SP} distances sampled with replacement from the set of distances among all neurons, where N_{SP} was the number of distances among SP neurons. The *P*-value was calculated as the fraction of Y^* values more extreme than Y. We used the same procedure for DP neurons.

Unless otherwise noted, we calculated confidence intervals using a nonparametric multistage bootstrap[58] method that simulates the data generation process and incorporates both variability among neurons for a given mouse and variability among mice. We calculated the confidence interval for statistic Y (for example, a mean hit – miss difference across mice) as follows, where Y was calculated using data from N mice, and where N_k is the number of neurons obtained from the kth mouse (we first pooled neurons collected in separate sessions for a mouse). First, mice were sampled randomly with replacement to obtain a set of N primary sampling units (PSUs). Next, N_k neurons were sampled with replacement for each PSU. A bootstrap replicate, Y^*, was calculated for each of 50,000 such bootstrap samples. The 95% confidence interval for Y was calculated as the 2.5th and 97.5th percentile values of Y^*.

We assigned mice of appropriate genotypes to experimental groups arbitrarily, without randomization or blinding. We did not use statistical methods to predetermine sample sizes. Sample sizes are similar to those reported in the field.

A **Supplementary Methods Checklist** is available.

Data availability. The data that support the findings of this study are available from the corresponding author upon request.

Code availability. Data analyses were conducted in MATLAB using scripts available from the corresponding author upon request.

51. Dana, H. *et al.* Thy1-GCaMP6 transgenic mice for neuronal population imaging in vivo. *PLoS One* **9**, e108697 (2014).
52. Hippenmeyer, S. *et al.* A developmental switch in the response of DRG neurons to ETS transcription factor signaling. *PLoS Biol.* **3**, e159 (2005).
53. Madisen, L. *et al.* A toolbox of Cre-dependent optogenetic transgenic mice for light-induced activation and silencing. *Nat. Neurosci.* **15**, 793–802 (2012).
54. O'Connor, D.H. *et al.* Neural coding during active somatosensation revealed using illusory touch. *Nat. Neurosci.* **16**, 958–965 (2013).
55. Pologruto, T.A., Sabatini, B.L. & Svoboda, K. ScanImage: flexible software for operating laser scanning microscopes. *Biomed. Eng. Online* **2**, 13 (2003).
56. O'Connor, D.H., Peron, S.P., Huber, D. & Svoboda, K. Neural activity in barrel cortex underlying vibrissa-based object localization in mice. *Neuron* **67**, 1048–1061 (2010).
57. Kerlin, A.M., Andermann, M.L., Berezovskii, V.K. & Reid, R.C. Broadly tuned response properties of diverse inhibitory neuron subtypes in mouse visual cortex. *Neuron* **67**, 858–871 (2010).
58. Davison, A.C. & Hinkley, D.V. *Bootstrap Methods and their Application* (Cambridge Univ. Press, 1997).